Kinematics and Dynamics of a Continuum Immobilization Mechanism for Frameless Cancer Radiotherapy

Olalekan Ogunmolu†, Xinmin Liu⋆, and Rodney Wiersma⋆

***Abstract*—TO-DO: Under development**

I. INTRODUCTION

This paper is a continuation of the constitutive model of a single soft robot, called IABs that we modeled and verified in [1] for use in real-time motion compensation/correction in radiation therapy. Here, we present the systematic analysis of the parallel continuum inflatable air bladders (IAB) which are surrogate manipulator of head and neck region of a patient in framless and maskless (F&M) immobilization during cranial radiosurgery or radiation therapy of the head and neck (H&N) region of a patient. Having a real-time closed-loop robotic system that can automatically correct motion deviation, particularly during beam-on time during RT treatment is a desperately needed technology that has the potential benefits of hastening the current treatment time in clinics, minimizing patient discomfort post treatment (as opposed to rigid frames and masks used in frame and mask-based RT), and drastically improve dose efficacy so that the patient's treatment can be effectively fractionated. For details on the radiation oncological treatment procedure, we refer readers to [2] and [3].

In this work, we derive the kinematics of a wearable soft continuum mechanism as described in [1] (figure reproduced in Figure 1) necessary for the immobilization, as well as planning and control of a patients' head and neck motion on a treatment machine. We call the individual soft robots inflatable air bladders (IABs) owing to their hollow internal chambers that admits air or ejects air based on an applied pressurization. Again, we make the fundamental assumption that the IAB's deformation follows the isochoric principle, with reasonable isochoric constraints baked into the physical IAB hardware, and we follow the model that we earlier derived in [1] in determining the manipulator's forward kinematics, Jacobian and its associated kinematic characteristics. Soft parallel robots are notoriously difficult to control, given their continuum-based mechanical properties, the inter-dependency of the parameters that characterize their deformation, and the individual robot constraints: the relative 3D orientation, permitted motion orientations, the 3D relation between constraints and allowed motions, and the possibility of multiple assembly modes that may result in the same end-effector pose [4]. It is not surprising that different schemes for controlling soft continuum robots have appeared in literature with mixed successes.

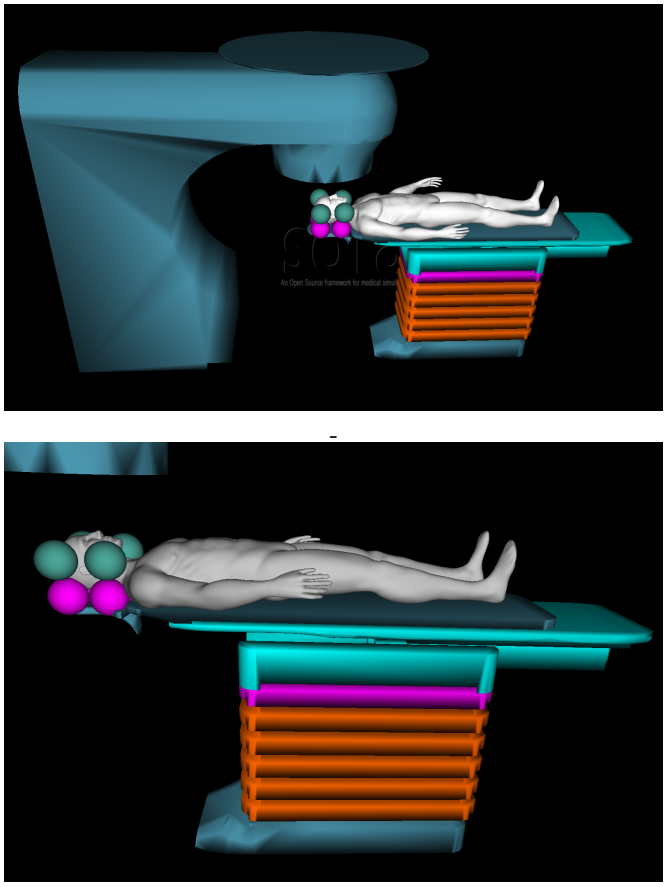

Fig. 1: System setup in the SOFA Framework Architecture. **Top**: Gantry, Turntable, Patient and IAB Chains around the patient's H&N Region. **Bottom**: Close-up view of compensating IABs around patient's H&N region with the patient lying in a supine position on the treatment couch.

The configurations we treat consists of soft robot links connected with extensible couplings; these couplings are chosen to exploit the soft structures' design for impedance control of the head and neck region of a patient. We analyze the manipulation map, kinematics of the respective IAB chains, and the contact equations and interaction between the IAB mechanism system and head. More importantly, we present

†Perelman School of Medicine, The University of Pennsylvania, Philadelphia, PA 19104, USA. ogunmolo@pennmedicine.upenn.edu

⋆Department of Radiation Oncology, The University of Chicago, Chicago, IL 60637, USA. {xmliu, epearson, rwiersma}@uchicago.edu

Research reported in this publication was supported by National Cancer Institute of the National Institutes of Health under award number R01CA227124

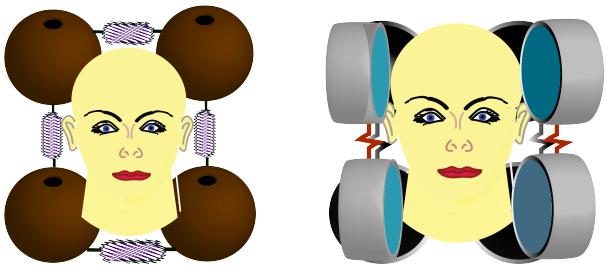

Fig. 2: An abstraction of the patient's position correction mechanism. In the left image, there are four IABs that constitute the base kinematic chain. They lift the head along the Z-axis as well as provide pitch motion corrections. On the right, the side kinematic chains provide roll and yaw motion corrections.

a sequel to the constitutive model which was derived in [1], and we expand upon the kinematic configuration of a multi-DOF soft actuation system for head and neck immobilization in RT. Our design goal is an immobilization system that provides comfort for the patient while manipulating human body parts, provides dose efficacy whilst providing for motion correction and a soft continuum actuation system that is able to emerge complex morphological computational behavior with soft deformable inflatable air bladders (IABs) that simplify complex patient motion control during robotic radiation therapy treatment.

TO-DO: The rest of this paper is organized as follows. In § II, we provide an overview of the system configuration, we then analyze the contact kinematics in § III; this includes our contact model, and how we solve the boundary value problem with the contact. In § IV, we derive the mechanism's manipulation map and Jacobian by solving for the its end-effector velocities and forces. We provide manipulation examples and results from our simulation in the SOFA framework in § V. We conclude the paper in § VIII.

II. A Soft Assembly for Patient Immobilization

Figure 2 shows the kinematic arrangement of the soft robots around the head. The geometry of this material has inflatable internal cavities that pressurize under the influence of fluids that flow via pneumatic hoses/tubes. The complete setup in a typical radiation oncology treatment room that includes the gantry, couches, turntable, as well as patient lying in a supine position on a treatment table is shown in Figure 1 as modeled in the SOFA Framework architecture [5]. The IABs are linked by semi-plastic connectors that allow for passive displacement and orientation to accommodate varying patient head sizes and shapes when one or more of the IABs deform. The system is composed of one closed and two open soft robot kinematic chains. The deformation from passive compliance of the chains can be easily measured, and the inherent elasticity of the rubber components increase passive compliance so that the controlled actuators can be used to generate a fixed behavior model.

The range of motions of the kinematic arrangement above give are described in what follows. Take the left symmetry of the robot configuration. This manipulates the cranial region about the $+x$ axis, while the right kinematic chain manipulates the head about the right-left plane($-x$). A 4-IAB closed kinematic chain lies underneath the patient's head, providing actuation about the anterior-posterior direction: they compensate the head along the z-axis or in a pitch orientation direction. When only two along the sides are actuated, it results in a yaw/y-axis motion of the head. We utilize the four pairs to realize precise translational and rotatory head motions about the z-axis. The connectors between the IABs in each chain are passive, adjustable to accommodate a patient's head size.

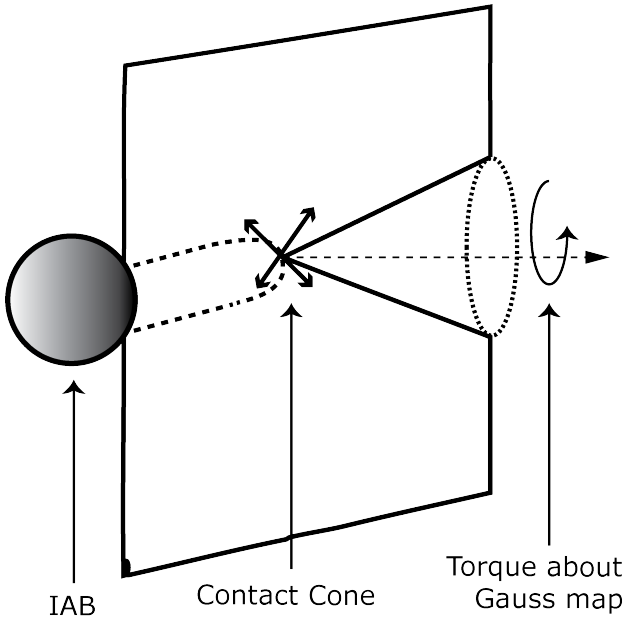

Fig. 3: Illustration of the IAB Soft Contact Type

III. Analysis of Contact Kinematics

We describe the contact between an IAB and the head through a mapping between the force exerted by the IAB at the contact point and the resultant forces at the center of mass of the head. We model the contact type between the head and an IAB similar to the soft finger contact primitive of [6]. Here, our soft contact is the convex sum of *point contacts* with friction over the small area of contact. IAB forces and torques are modeled within a "cone of forces" about the direction of the surface normal from a patient's head (see Figure 3). The trajectory of the head under the influence of motion of an IAB is influenced by the position vector $\mathbf{r}$ described in [1]. When the IAB deforms, body forces over its current configuration and contact (*traction*) forces over its boundary $\partial\mathcal{B}$ impact motion on the head. Constrained by the frictional coefficient, we define the soft contact force inside the friction cone as

$$\tilde{F}_{c_i} = \begin{bmatrix} \mathbf{I} & 0 \\ 0 & n_{c_i} \end{bmatrix} \begin{bmatrix} f_{c_i} \\ \tau_{c_i} \end{bmatrix}, \tag{1}$$

where $f_{c_i} \in \mathbb{R}^3$ denotes the amount of force exerted by the IAB along the direction of contact, $\tau_{c_i} \in \mathbb{R}$ is the moment of the contact force, and n_{c_i} is the *normal map* or *Gauss map*[1]

[1]A normal map for a manifold S is a continuous map $g : S \to S^2 \subset \mathbb{R}^3$such that for every $s \in S$, $g(s)$ is orthogonal to S at s [7].

for a manifold $S \subset \mathbb{R}^3$ of a head surface. For contact models with friction, we require that all contact forces lie within the friction cone, determined by the friction coefficient. The set of forces within or on the boundary of the friction cone is

$$FC = \{f_c \in \mathbb{R}^n : \|f^t_{c_{ij}}\| \leq \mu_{ij}\|f^n_{c_i}\|, \\ i = 1, \ldots, k,\ j = 1, \ldots, m_i\} \tag{2}$$

where $f^t_{c_{ij}}$ is the tangent component of the j^{th} element of the contact force, $f^n_{c_i}$ is i^{th} contact's normal force, and μ_{ij} is $f_{c_{ij}}$'s coefficient of friction.

A. Contact-Based Boundary Value Problem for IAB

We now solve the boundary-value problem for the IAB deformation when in contact with the head as a follow-up to our analysis in [1]. Again, we assume a spherically-symmetric deformation constraint imposed on the IAB when the head rolls or slips. This may be achieved through an appropriate vulcanization of the IAB rubber material, for example (see [8] or [9]). For a semi-rigid IAB material, when the SoRos are in contact with the head, the applied forces on the current configuration of the IAB body $\mathcal{B}$ are

- the body forces, $\boldsymbol{b}$
- the contact forces, f_c, at the IAB boundary, $\partial\mathcal{B}$, and
- the gravitational force of the head mass acting along the direction of contact, f_g.

We make the explicit assumption that the head maintains contact with the IAB throughout deformation. Suppose that for the i^{th} IAB in the chain, r_{c_i} represents the direction vector perpendicular from the point of contact to the center of the head cone of forces, it follows that the three equations that governs the motion of the IAB continuum are given as

$$\dot{\rho} + \rho \operatorname{div} \mathbf{v} = 0 \tag{3a}$$

$$\boldsymbol{\sigma}^T = \boldsymbol{\sigma} \tag{3b}$$

$$\operatorname{div} \boldsymbol{\sigma}^T + \rho \boldsymbol{b} = \rho \dot{\mathbf{v}}, \tag{3c}$$

being respectively the conservation of mass (3a), the symmetry of the stress tensor (3b), and the balance of linear momentum respectively, (see [10, pp. 150], for the derivation). In general, we expect that the mass of the body will be conserved given the incompressibility assumption of the IAB material, thus guaranteeing that (3a) is fulfilled. We have from (3c) and the symmetric properties of the stress tensor that

$$\frac{1}{r^2}\frac{\partial}{\partial r}(r^2\sigma_{rr}) + \frac{1}{r\sin\phi}\frac{\partial}{\partial\phi}(\sin\phi\sigma_{r\phi}) + \frac{1}{r\sin\phi}\frac{\partial}{\partial\theta}(\sigma_{r\theta}) \\ - \frac{1}{r}(\sigma_{\theta\theta} + \sigma_{\phi\phi}) + \rho b_r \rho\ddot{\mathbf{r}}_x \tag{4a}$$

$$\frac{1}{r^3}\frac{\partial}{\partial r}(r^3\sigma_{r\phi}) + \frac{1}{r\sin\phi}\frac{\partial}{\partial\phi}(\sin\phi\sigma_{\phi\phi}) + \frac{1}{r\sin\phi}\frac{\partial}{\partial\theta}(\sigma_{\theta\phi}) \\ - \frac{\cot\phi}{r}(\sigma_{\theta\theta}) + \rho b_\phi = \rho\ddot{\mathbf{r}}_y \tag{4b}$$

$$\frac{1}{r^3}\frac{\partial}{\partial r}(r^3\sigma_{\theta r}) + \frac{1}{r\sin^2\phi}\frac{\partial}{\partial\phi}(\sin^2\phi\sigma_{\theta\phi}) \\ + \frac{1}{r\sin\phi}\frac{\partial}{\partial\theta}(\sigma_{\theta\theta}) + \rho b_\theta = \rho\ddot{\mathbf{r}}_z \tag{4c}$$

where $\ddot{\mathbf{r}}_x, \ddot{\mathbf{r}}_y$, and $\ddot{\mathbf{r}}_z$ are components of the position vector $\ddot{\mathbf{r}}$ as defined in Appendix B of [2] and the body forces b_r, b_ϕ, b_θ are components of the gravitational force of the head acting on the IAB body $\boldsymbol{B}$. If the deformation is spherically symmetric, we expect that the shear stress component contributions $\sigma_{r\phi}, \sigma_{r\theta}, \sigma_{\phi\theta}$ would vanish in (4). It follows that the forces on the head (see derivation in Appendix C of [11]) are in part the internal pressurization, and component stresses $\{P_i, \sigma_{\phi\phi}(\epsilon), \sigma_{\theta\theta}(\zeta)\}$ as given in (5)

$$P = \int_{r_i}^{r_\circ} \Big[\frac{1}{r}\left(-2p + 2C_1\frac{r^2}{R^2} - 2C_2\frac{R^8}{r^8}\right) - \rho b_r \\ + \rho\cos\theta\left(2\dot{r}\dot{\phi}\cos\theta + r\cos\theta\ddot{\phi} - 2r\dot{\theta}\dot{\phi}\sin\theta\right) - \rho\sin\phi \\ \left(\cos\theta(-\ddot{r} + r\dot{\theta}^2 + r\dot{\phi}^2) + \sin\theta(2\dot{r}\dot{\theta} + r\ddot{\theta})\right)\Big]\, dr \tag{5a}$$

$$\sigma_{\phi\phi}(\epsilon) = -\int_\epsilon^\pi \Big[r\rho\Big[\cos\phi\left(2r\dot{\theta}\dot{\phi}\cos\theta + (2\dot{r}\dot{\phi} + r\ddot{\phi})\sin\theta\right) \\ + \sin\theta\left(2\dot{r}\dot{\theta}\cos\theta + r\ddot{\theta}\cos\theta + (\ddot{r} - r\dot{\theta}^2 - r\dot{\phi}^2)\right)\sin\phi\Big] \\ - \rho r b_\theta\Big]\, d\phi,\ 0 \leq \epsilon \leq \pi \tag{5b}$$

$$\sigma_{\theta\theta}(\zeta) = -\int_\zeta^{2\pi} \Big[-r\rho b_\theta\sin\phi + r\rho\sin\phi\cos\phi\left(\ddot{r} - r\dot{\phi}^2\right) \\ - r\rho\sin^2\phi\left(2\dot{r}\dot{\phi} + r\ddot{\phi}\right)\Big]\, d\theta,\ 0 \leq \zeta \leq 2\pi, \tag{5c}$$

where $0 \leq \epsilon \leq \pi$, and $0 \leq \zeta \leq 2\pi$.

B. Contact Forces, IAB Stress Components, and Head Gravitational Force

We assume that the stress vector $\boldsymbol{\sigma}$ at a point on the IAB surface is uniform and continuous throughout the IAB boundary so that it linearly depends on the normal map (this follows from Cauchy's theorem; readers may see the proof in [10, §3.3.1]). Recall that the correspondence between material line elements in the reference and current configuration is

$$\mathbf{dx} = \mathbf{F}\ \mathbf{dX} \quad \Longrightarrow \quad \mathbf{F}^{-T}\mathbf{dx} = \mathbf{dX}.$$

Let $\mathbf{H} = \mathbf{F}^{-T}$ and $\mathbf{dA}$ represent an infinitesimal vector element on the material surface at a neighborhood of point $\mathbf{X}$ in $\mathcal{B}$ such that $\mathbf{dA} = \mathbf{N}\mathrm{dA}$, where $\mathbf{N}$ is the unit outward normal to the IAB boundary $\partial\mathcal{B}_\circ$ in the reference configuration. The corresponding deformed surface of the IAB with normal $\mathbf{n}$ from a surface, da, of the IAB in the current configuration is $\mathbf{da} = \mathbf{n}\,\mathrm{da}$. Using *Nanson's formula*, we have the following relation between surfaces in the reference and current configuration

$$\mathbf{da} = J\,\mathbf{H}\ \mathbf{dA} \quad \Longrightarrow \quad \mathbf{n}\,\mathrm{da} = J\,\mathbf{H}\ \mathbf{N}\ \mathrm{dA}. \tag{6}$$

where $J = \det\mathbf{F}$. Multiplying throughout equation (6) by the derived constitutive relation between the stress-strain relationship of [1], the resultant contact force on the boundary $\partial\mathcal{B}$ in the current configuration may be written as (owing to the volume preservation on the boundary of the IAB material)

$$\int_{\partial\mathcal{B}} \boldsymbol{\sigma}\,\mathbf{n}\,\mathrm{da} = \int_{\partial\mathcal{B}_\circ} J\,\boldsymbol{\sigma}\,\mathbf{H}\mathbf{N}\ \mathrm{dA}. \tag{7}$$

The *Piola-Kirchoff* stress tensor field is defined as

$$\mathbf{S} = J\,\mathbf{H}^T\,\boldsymbol{\sigma}. \tag{8}$$

(see [10, §4.2]). It follows that the force on an element surface da of the IAB in a configuration $\mathcal{B}$ is

$$\boldsymbol{\sigma}\mathbf{da} = \mathbf{S}^T\mathbf{dA}.$$

Thus, the contact force f_{c_i} on the boundary $\partial\mathcal{B}$ of the i^{th} IAB in a configuration $\mathcal{B}$ (as in (1)) is

$$f_{c_i} = \mathbf{S}_i^T\mathbf{dA}_i = J_i\boldsymbol{\sigma}_i\mathbf{H}_i\mathbf{dA}_i = J_i\boldsymbol{\sigma}_i\mathbf{F}_i^{-1}\mathbf{dA}_i \tag{9}$$

where (9) follows from the symmetric property of $\mathbf{F}_i$ and $\boldsymbol{\sigma}_i$. For the i^{th} IAB, at the region of contact, we have the contact force as

$$f_{c_i} = J_i\left(\frac{R_i^2}{r_i^2}P_i + \frac{R_i}{r_i}\sigma_{\phi\phi_i}(\epsilon) + \frac{R_i}{r_i}\sigma_{\theta\theta_i}(\zeta)\right)\mathbf{dA}_i \tag{10}$$

where $\sigma_{jj_i}(\upsilon)$ are the definite integrals of (5). Owing to the isochoric deformation assumption, we have from (10) that

$$f_{c_i} = \left(\frac{R_i^2}{r_i^2}P_i + \frac{R_i}{r_i}\sigma_{\phi\phi_i}(\epsilon) + \frac{R_i}{r_i}\sigma_{\theta\theta_i}(\zeta)\right)n_{c_i}dA_i. \tag{11}$$

where we have set the outward normal map $\mathbf{N}$ to n_{c_i} of (1). The torque is the moment of the contact force on the i^{th} IAB,and it is given by

$$\boldsymbol{\tau}_{c_i} = f_{c_i} \times r_{c_i} \tag{12}$$

where $r_{c_i} \in \mathbb{R}^3$ is the unit vector between the head reference point and the contact. The soft contact force of (1) can be re-stated in terms of the derived stress tensor, the deformation gradient (see [1]) and the Piola-Kirchoff stress field of (8) *i.e.*

Friction Cones' Contact Force

$$\tilde{F}_{c_i} = \begin{bmatrix}\mathbf{I} & 0\\ 0 & n_{c_i}\end{bmatrix}\begin{bmatrix}f_{c_i}\\ f_{c_i}\times r_{c_i}\end{bmatrix}. \tag{13}$$

where f_{c_i} and $\boldsymbol{\tau}_{c_i}$ are as given in equations (11) and (12).

C. Contact Coordinates and Head Velocity

The head will make contact with the IAB at multiple points on its surface, so we describe the kinematics of these contact points using an atlas[2] of contact coordinate charts. In this sentiment, let C_{r_1} and C_{r_h} respectively represent a fixed reference frame with respect to the IAB and head, H (see Figure 4). Furthermore, let $S_1 \subset \mathbb{R}^3$ and $S_h \subset \mathbb{R}^3$ denote the respective *orientable manifold*[3] embeddings of the IAB and head surfaces with respect to frames C_{r_1} and C_{r_h}. We shall let S_1 and S_r belong to the *atlases* $\{S_{1_i}\}_{i=1}^{n_1}$, $\{S_{h_i}\}_{i=1}^{n_r}$ respectively. Suppose (f_1, U_1) and (f_r, U_r) are *coordinate*

[2]An atlas $\tilde{S}$ is a set of surfaces where each surface $S \in \tilde{S}$ has an invertible map $f(\boldsymbol{u})$ from an open subset U of $\mathbb{R}^2$ to a surface $S \subset \mathbb{R}^3$ such that the partial derivatives $\frac{\partial f}{\partial u}(\boldsymbol{u})$, $\frac{\partial f}{\partial v}(\boldsymbol{v})$ are linearly independent for all $\boldsymbol{u} = (u, v) \in U$.

[3]An orientable manifold is a manifold S for which the Gauss map exists.

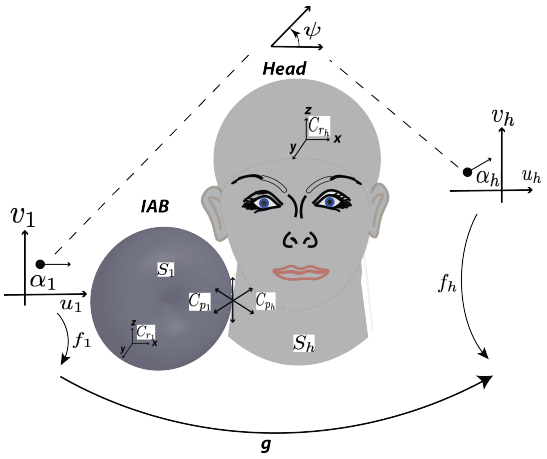

Fig. 4: Sliding and rolling contact illustration of a single IAB and the Head

systems for the IAB and the head respectively, where f_i is an invertible map, $f_i(u_i, v_i) : U \to S_i \subset \mathbb{R}^3$

$$f_i(u_i, v_i) : \{U \to S_i \subset \mathbb{R}^3 | i = 1, h\},$$

from an open subset U of $\mathbb{R}^2$ to a *coordinate patch* $S_i \subset \mathbb{R}^3$ such that the partial derivatives $\frac{\partial f_i}{\partial u_i}$ and $\frac{\partial f_i}{\partial v_i}$ are linearly independent. Let $p_1(t) \in S_1$ and $p_h(t) \in S_h$ represent the positions of the contact points with respect to frames C_{r_1} and C_{r_h} respectively at time t. In general, the contact points $p_1(t)$ and $p_h(t)$ will not remain in the coordinate systems S_1 and S_h for all time. Thus, we choose an interval I where $p_1(t) \in S_{1_i}$ and $p_h(t) \in S_{h_j}$ for all $t \in I$ and some i and j. As seen in Figure 4, C_{p_1} and C_{p_h} denote the contact frames that coincide with the *normalized Gauss frames* at p_1 and p_h for all $t \in I$, and α_1, α_h are local coordinate frames that describe the IAB motion with respect to the head such that

$$\alpha_1 = (u_1, v_1) \in U_1, \text{ and } \alpha_h = (u_h, v_h) \in U_h.$$

Let the angle between the tangent planes of α_1, and α_h be ψ. The transformation matrix $g \in \Omega \subset SE(3)$ encodes the relative orientation and position of the IAB with respect to the head where Ω is the set of all relative positions and orientations in the atlasses $\{S_{1_i}\}_{i=1}^{n_1}$, $\{S_{h_i}\}_{i=1}^{n_h}$ for which the IAB and head remain in contact. We let the *contact coordinates* be described by $\eta = (\alpha_1, \alpha_h, \psi)$. The head's motion is governed by traction forces arising from the friction tangential to the IAB surface and the pressure normal to the IAB surface. Thus, at the points of contact, if $R \in SO(3)$ is the rotatory component of g, η must satisfy

$$g \circ f_1(\alpha_1) = f_h(\alpha_h) \tag{14a}$$

$$R\,n_1(\alpha_1) = -n_h(\alpha_h) \tag{14b}$$

since the contact locations must coincide for the IAB and the head, and the tangent planes must coincide so that the outward normal maps $n_1 : S_1 \to S^2 \subset \mathbb{R}^3$ and $n_h : S_h \to S^2 \subset \mathbb{R}^3$ agree. Furthermore, the orientation of the tangent planes of α_1 and α_h is the unique angle $\psi \in [0, 2\pi)$ between the x-axes of

C_{p_1} and C_{p_h} such that

$$R\frac{\partial f_1}{\partial \alpha_1}M_1^{-1}R_\psi = \frac{\partial f_h}{\partial \alpha_h}M_h^{-1} \tag{15}$$

where M_i is a 2×2 square root of the Riemannian metric tensor [12] that normalizes the columns of $\frac{\partial f}{\partial \alpha}$, *i.e.*

$$M_i = \begin{bmatrix} \|\frac{\partial f_i}{\partial u_i}\| & 0 \\ 0 & \|\frac{\partial f_h}{\partial v_i}\| \end{bmatrix} \tag{16}$$

and R_ψ is chosen such that a rotation of C_{p_1} about its z-axis through $-\psi$ radians aligns the x-axes of the local coordinate system α_1 to that of the head's local coordinate system α_h *i.e.*

$$R_\psi = \begin{bmatrix} \cos\psi & -\sin\psi \\ -\sin\psi & -\cos\psi \end{bmatrix}. \tag{17}$$

Notice that $R_\psi = R_\psi^T = R_\psi^{-1}$. We define the normalized Gauss frame at a point u on the surface U of the orthogonal coordinate system (f, U) as,

$$\begin{bmatrix} x_u & y_u & z_u \end{bmatrix} = \begin{bmatrix} \frac{\partial f}{\partial u}/\|\frac{\partial f}{\partial u}\| & \frac{\partial f}{\partial v}/\|\frac{\partial f}{\partial v}\| & n_u(f(u)) \end{bmatrix} \tag{18}$$

where x_u, y_u, and z_u are functions mapping $U \subset \mathbb{R}^2 \to \mathbb{R}^3$ and n_u is the continuous Gauss map $n_u : S \to S^2 \subset \mathbb{R}^3$. The motion of the contacts $\dot{\eta}$ as a function of components of the twist vector $\hat{\xi} = (v, w)^T$ is given in (19) as the respective *first, second*, and *third equations of contact*. Our derivation, which closely follows [13]'s multi-fingered kinematics' proof, may be found in Appendix B of [2].

$$\dot{\alpha}_h = M_h^{-1}(\mathcal{K}_h + \tilde{\mathcal{K}}_1)^{-1}\left(\omega_t - \tilde{\mathcal{K}}_1 v_t\right) \tag{19a}$$

$$\dot{\alpha}_1 = M_1^{-1}R_\psi(\mathcal{K}_h + \tilde{\mathcal{K}}_1)^{-1}\left(\omega_t - \mathcal{K}_h v_t\right) \tag{19b}$$

$$\dot{\psi} = \omega_n + T_h M_h \dot{\alpha}_h + T_1 M_1 \dot{\alpha}_1 \tag{19c}$$

where

$$T_h = y_h^T \frac{\partial x_h}{\partial \alpha_h}M_h^{-1}, \quad T_1 = y_1^T \frac{\partial x_1}{\partial \alpha_1}M_1^{-1},$$

$$\mathcal{K}_h = \begin{bmatrix} x_h^T, & y_h^T \end{bmatrix}^T \frac{\partial n_h^T}{\partial \alpha_h}M_h^{-1}, \quad \omega_n = z_h^T \omega$$

$$\mathcal{K}_1 = R_\psi \begin{bmatrix} x_1^T, & y_1^T \end{bmatrix}^T \frac{\partial n_1^T}{\partial \alpha_1}M_1^{-1}R_\psi,$$

$$\omega_t = \begin{bmatrix} x_h^T, & y_h^T \end{bmatrix}^T \begin{bmatrix} n_h \times \omega \end{bmatrix}^T,$$

$$v_t = \begin{bmatrix} x_h^T, & y_h^T \end{bmatrix}^T \begin{bmatrix} (-f_h \times \omega + v) \end{bmatrix}^T. \tag{20}$$

Note that ω_t is the rolling velocity of the head projected onto the tangent plane of the contact and v_t is the sliding velocity; ω_n is the relative rotational velocity projected to the contact's surface normal, and $\tilde{\mathcal{K}}_1 = R_\psi \mathcal{K}_1 R_\psi$ is the curvature of the IAB with respect to the contact frame that coincides with the normalized Gauss frame at $p_1(t)$. The matrix $(\mathcal{K}_h + \tilde{\mathcal{K}}_1)^{-1}$ is the so-called *relative curvature* originally coined by [7].

Simplifying (20), we find that

$$x_h = \frac{\partial f}{\partial u_h}/\|\frac{\partial f}{\partial u_h}\|, \quad y_h = \frac{\partial f}{\partial v_h}/\|\frac{\partial f}{\partial v_h}\|, \qquad z_h = n_u(f(u))$$

$$T_h = y_h \left[\frac{\partial x_h^T}{\partial u_h}/\|\frac{\partial f}{\partial u_h}\|, \frac{\partial x_h^T}{\partial v_h}/\|\frac{\partial f}{\partial v_h}\|\right],$$

$$T_1 = y_1 \left[\frac{\partial x_1^T}{\partial u_1}/\|\frac{\partial f}{\partial u_1}\|, \frac{\partial x_1^T}{\partial v_1}/\|\frac{\partial f}{\partial v_1}\|\right],$$

$$\mathcal{K}_h = \begin{bmatrix} x_h^T, & y_h^T \end{bmatrix}^T \left[\frac{\partial n_h^T}{\partial u_h}/\|\frac{\partial f}{\partial u_h}\|, \frac{\partial n_h^T}{\partial v_h}/\|\frac{\partial f}{\partial v_h}\|\right],$$

$$\mathcal{K}_1 = \begin{bmatrix} x_1^T, & y_1^T \end{bmatrix}^T \left[\frac{\partial n_1^T}{\partial u_1}/\|\frac{\partial f}{\partial u_1}\|, \frac{\partial n_1^T}{\partial v_1}/\|\frac{\partial f}{\partial v_1}\|\right]. \tag{21}$$

We see that for the contact interaction between an IAB and the head, for a $U \subset \mathbb{R}^2$ we must choose an appropriate $f_i : U_i \to S_i \subset \mathbb{R}^3$ in order to characterize the setup.

IV. Multi-IAB Kinematics

At a material point, $\mathbf{r}$, of the IAB surface in the configuration $\mathcal{B}$, the 3D position of a point based on the radial distance r from the origin and the angles ϕ and

$$\mathbf{R} = \begin{bmatrix} R\cos\Theta\sin\Phi, \\ R\sin\Theta\sin\Phi, \\ R\cos\Phi \end{bmatrix} \quad \text{and} \quad \mathbf{r} = \begin{bmatrix} r\cos\theta\sin\phi, \\ r\sin\theta\sin\phi, \\ r\cos\phi \end{bmatrix}. \tag{22}$$

θ is given by (22). The configuration space of the IAB with respect to the spatial frame at a certain time can then be described by $g_{st}(\mathbf{r}) : \mathbf{r} \to g_{st}(\mathbf{r}) \in SE(3)$ while the strain state of the IAB is characterized by the strain field

$$\hat{\xi}_i(\mathbf{r}) = g_i^{-1}\frac{\partial g_i}{\partial \mathbf{r}} \in \mathfrak{se}(3) = g_i^{-1}g_i' \tag{23}$$

with the respective g_i's being the tangent vector at g_i such that $g_i' \in T_{g_i(\mathbf{r})}SE(3)$. For an incompressible IAB, the strain field becomes

$$g_i(\mathbf{r}) = \exp^{\|\mathbf{r}\|\hat{\xi}_i} = \mathbf{I} + \hat{\xi}_i\|\mathbf{r}\| + \frac{\hat{\omega}}{\|\omega\|^2}\left(1 - \cos(\|\mathbf{r}\|\|\omega\|)\right)\hat{\xi}_i^2 + \frac{\hat{\omega}^3}{\|\omega\|^3}\left(\|\mathbf{r}\|\|\omega\| - \sin(\|\mathbf{r}\|\|\omega\|)\right)\hat{\xi}_i^3. \tag{24}$$

A. End Effector Forces

From the derived relationship between the head contact coordinates and the relative motion (v_t, ω_t) of the IAB *i.e.* equation (19), we can associate a Jacobian that maps IAB velocities to head position and orientation. A basic assumption in our formulation is that the IABs make contact with the head throughout manipulation, and the manipulation is stable and prehensile. A forward kinematic map $K_{iab_i}(\mathbf{r}_i) : \mathbb{R}^{n_i} \to SE(3)$ maps from respective IAB positions to head position and orientation. The velocity of the head with respect to a fixed base frame in terms of IAB velocities can be written in terms of the forward kinematics Jacobian:

$$\begin{pmatrix} v_{iab_i} \\ \omega_{iab_i} \end{pmatrix} = \frac{\partial K_{iab_i}}{\partial \mathbf{r}_i}\frac{d\mathbf{r}}{dt}K_{iab_i}^{-1} = \boldsymbol{J}_i(\mathbf{r}_i)\dot{\mathbf{r}}_i \tag{25}$$

where $\mathbf{r}_i$ is the spatial position of IAB i, and $(v_{iab_i}^T, \omega_{iab_i}^T) \in \mathbb{R}^6$ represents the linear and angular velocity of the i^{th} IAB about its screw basis. In essence, $\mathbf{r}_i \in \mathbb{R}^3$ with its rows of mapped to

scalars by an appropriate choice of norm. The contact between the head and the IABs is mapped by the Jacobian

$$\boldsymbol{J}_{c_i}(\xi_h, \xi_{iab_i}) = \begin{bmatrix} \mathbf{I} & \hat{\boldsymbol{w}}(r_{c_i}) \\ \mathbf{0} & \mathbf{I} \end{bmatrix} J_{r_i}, \tag{26}$$

where $\boldsymbol{J}_{c_i} : \dot{\xi}_{r_i} \to \begin{bmatrix} v_{c_i}^T, & w_{c_i}^T \end{bmatrix}^T$, $r_{c_i} \in \mathbb{R}^3$ is a vector between the head reference point (e.g. the center of mass) and the contact with the i^{th} IAB, ξ_h is the position and relative orientation of the head, ξ_{iab_i} is the position and relative orientation of the i^{th} soft robot in world coordinates, $\hat{\boldsymbol{w}}(r_{c_i})$ is an anti-symmetric matrix for the vector r_{c_i}, and $\xi_r = (\xi_{r_1}, \xi_{r_2}, \cdots, \xi_{r_8})$ are the positions and orientations for each of the 8 IABs. The manipulation map, G_i is made up of matrices of the form

$$G_i(\xi_h, \xi_r) = \begin{bmatrix} \mathbf{I} & \mathbf{0} \\ \hat{w}(r_{c_i}) & \mathbf{I} \end{bmatrix} B_i(\xi_h, \xi_r), \tag{27}$$

where $B_i(\xi_h, \xi_r)$ is the selection map as defined in [14] for the desired manipulation. The net force on the head is a sum of the individual forces arising from each IAB. Owing to the linearity of each individual IAB's contact force, the resultant head force can be stitched together to form G, *i.e.*

$$\tilde{F}_h = \begin{bmatrix} G_1, \ldots, G_8 \end{bmatrix} \begin{pmatrix} \tilde{F}_{c_1} \\ \vdots \\ \tilde{F}_{c_8} \end{pmatrix} = G\tilde{F}_c, \tag{28}$$

where $F_h \in \mathbb{R}^6$ and $F_c \in \mathbb{R}^{m_1} \times \mathbb{R}^{m_2} \times \ldots \times \mathbb{R}^{m_8}$. The *internal* or *null forces* is captured by the null space $\mathcal{N}(G)$ of the manipulation map G; these forces correspond to zero net force on the head of the patient. Each $\tilde{F}_{c_i}$ in (28) is of the form (13).

B. End-effector Velocities

Following [13], we define the velocity constraint dual of (27) as the constraint between the relative velocity of the head and that of the twist velocities of the contact point

$$\begin{pmatrix} \tilde{v}_{c_i} \\ \tilde{\omega}_{c_i} \end{pmatrix} = \begin{bmatrix} \mathbf{I} & \hat{\omega}(r_{c_i}) \\ 0 & \mathbf{I} \end{bmatrix} \begin{pmatrix} v_{c_h} \\ \omega_{c_h} \end{pmatrix}. \tag{29}$$

For a conjugate twist vector $(v_c^T, \omega_c^T)^T$ to the the forces exerted by the IABs, f_c, we have the following

$$\begin{pmatrix} v_c \\ \omega_c \end{pmatrix} = G^T \begin{pmatrix} v_{c_h} \\ \omega_{c_h} \end{pmatrix}. \tag{30}$$

Given a *selection matrix* $B_i^T(\xi_h, \xi_{iab_i}) \in \mathbb{R}_i^m$ for a particular manipulation task, where m_i is the range of all the forces and moments for the chosen contact primitive (or union of contact primitives), the *manipulation map* for the i^{th} IAB can be written as,

$$G_i^T(\xi_h, \xi_{iab_i})\xi_h = B_i^T(\xi_h, \xi_{iab_i})\boldsymbol{J}_{c_i}(\xi_h, \mathbf{r}_{r_i})\dot{\xi}_{iab_i} \tag{31}$$

where $\boldsymbol{J}_{c_i}$ is the contact Jacobian for the i^{th} soft robot, and ξ_h denotes the velocity of the head. In the arrangement of Figure 2, for the 8 soft robots, the manipulation constraint of

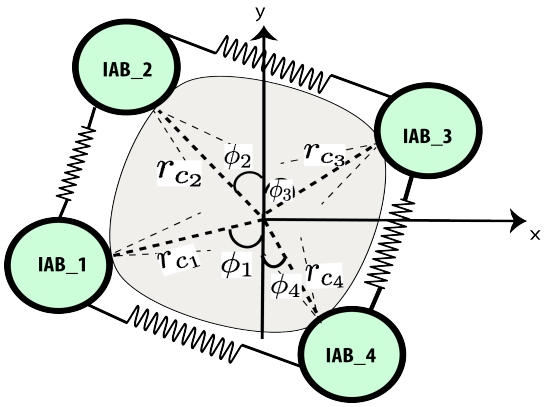

Fig. 5: Planar head manipulation with net force on the head.

the system can be written as

$$\begin{bmatrix} G_1^T \\ G_2^T \\ \vdots \\ G_8^T \end{bmatrix} \begin{pmatrix} v_h \\ w_h \end{pmatrix} = \mathbf{diag} \begin{pmatrix} B_1^T \boldsymbol{J}_{c_1} \\ B_2^T \boldsymbol{J}_{c_2} \\ \vdots \\ B_8^T \boldsymbol{J}_{c_8} \end{pmatrix} \begin{pmatrix} \dot{\mathbf{r}}_{iab_1} \\ \dot{\mathbf{r}}_{iab_2} \\ \vdots \\ \dot{\mathbf{r}}_{iab_8} \end{pmatrix}. \tag{32}$$

In what follows below, we give examples of the composition of the head manipulation map under different scenarios on a treatment table. These would be helpful when we use (31) to determine the head velocity in world coordinates. In these examples, there is an implicit assumption that the angle of tilt of the head around the axis of normal is measurable by a gyroscope or a vision sensor or other sensors of similar facsimile. We show how to find the manipulation map of the head when the IAB kinematic chain underneath the head are passive, and only the four IABs surrounding the head are actuated (see Figure 2) *i.e.* roll motion of the head. We then present finding the manipulation map of th ehead when all 8 IABs are simultaneously active *i.e.* the pitch, roll and yaw motion of the head.

V. IAB Kinematics Jacobian: Case Studies

A. Case I: Planar and Roll Manipulation

Consider a planar manipulation of the head as shown in Figure 5. Again, we use the cone of forces to model a *point contact* [6] between the head and soft robots. In this case, the robots beneath the head are passive while the side robots are actuated. For each IAB, the orientation of the vector r_{c_i} with respect to the vertical, measured counterclockwise is ϕ_i when the head lies on the xy plane; the manipulation matrix maps IAB forces into x and y forces as well as a torque perpendicular to the xy plane. We have the manipulation map as

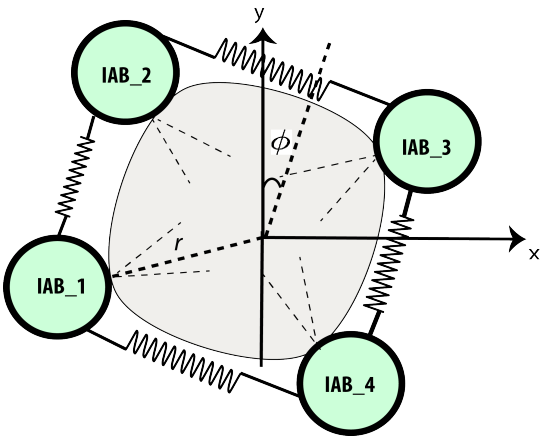

Fig. 6: Planar head manipulation with no net force on the head.

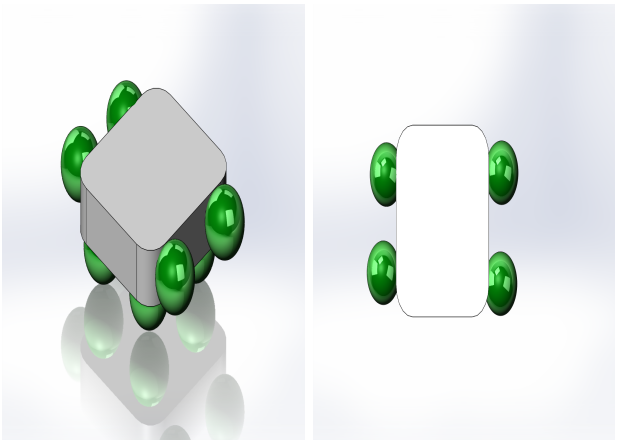

Fig. 7: Head manipulation with all eight bladders. Head depicted with the silver-colored solid.

$$G_1 = \begin{bmatrix} \mathbf{I} & 0 \\ \hat{\omega}\begin{pmatrix} -r_{c_1}\sin\phi_1 \\ -r_{c_1}\cos\phi_1 \\ 0 \end{pmatrix} & \mathbf{I} \end{bmatrix} \begin{pmatrix} 1 & 0 \\ 0 & 1 \\ 0 & 0 \\ 0 & 0 \\ 0 & 0 \\ 0 & 0 \end{pmatrix},$$

$$G_2 = \begin{bmatrix} \mathbf{I} & 0 \\ \hat{\omega}\begin{pmatrix} -r_{c_2}\sin\phi_2 \\ r_{c_2}\cos\phi_2 \\ 0 \end{pmatrix} & \mathbf{I} \end{bmatrix} \begin{pmatrix} 1 & 0 \\ 0 & 1 \\ 0 & 0 \\ 0 & 0 \\ 0 & 0 \\ 0 & 0 \end{pmatrix}$$

$$G_3 = \begin{bmatrix} \mathbf{I} & 0 \\ \hat{\omega}\begin{pmatrix} r_{c_3}\sin\phi_3 \\ r_{c_3}\cos\phi_3 \\ 0 \end{pmatrix} & \mathbf{I} \end{bmatrix} \begin{pmatrix} 1 & 0 \\ 0 & 1 \\ 0 & 0 \\ 0 & 0 \\ 0 & 0 \\ 0 & 0 \end{pmatrix},$$

$$G_4 = \begin{bmatrix} \mathbf{I} & 0 \\ \hat{\omega}\begin{pmatrix} r_{c_4}\sin\phi_4 \\ -r_{c_4}\cos\phi_4 \\ 0 \end{pmatrix} & \mathbf{I} \end{bmatrix} \begin{pmatrix} 1 & 0 \\ 0 & 1 \\ 0 & 0 \\ 0 & 0 \\ 0 & 0 \\ 0 & 0 \end{pmatrix} \tag{33}$$

whereupon, the planar manipulation map for the head becomes

$$G(x,y,\phi) = \begin{bmatrix} 1 & 0 & r_{c_1}\cos\phi_1 \\ 0 & 1 & -r_{c_1}\sin\phi_1 \\ 1 & 0 & -r_{c_2}\cos\phi_2 \\ 0 & 1 & -r_{c_2}\sin\phi_2 \\ 1 & 0 & -r_{c_3}\cos\phi_3 \\ 0 & 1 & r_{c_3}\sin\phi_3 \\ 1 & 0 & r_{c_4}\cos\phi_4 \\ 0 & 1 & r_{c_4}\sin\phi_4 \end{bmatrix}^T \tag{34}$$

for all forces with respect to the xy coordinates shown in Figure 5.

B. Case II: Planar Manipulation: Null Map for Zero Net Force

Now consider the case where all the vectors between each IAB in the xy plane and the head have equal magnitude such that the angle made by the head with respect to the vertical axis (y) is ϕ (see Figure 6). The head rolls around the vertical by an angle ϕ as shown. It follows that the manipulation map is

$$G_i(x,y,\phi) = \begin{bmatrix} \mathbf{I} & 0 \\ \hat{\omega}\begin{pmatrix} \pm r\sin\phi \\ \pm r\cos\phi \\ 0 \end{pmatrix} & \mathbf{I} \end{bmatrix} \begin{pmatrix} 1 & 0 \\ 1 & 0 \\ 0 & 0 \\ 0 & 0 \\ 0 & 0 \\ 0 & 0 \end{pmatrix} \tag{35}$$

so that

$$G(x,y,\phi) = \begin{bmatrix} 1 & 0 & 1 & 0 & 1 & 0 \\ 0 & 1 & 0 & 1 & 0 & 1 \\ r\cos\phi & -r\sin\phi & -r\cos\phi & -r\sin\phi & -r\cos\phi & r\sin\phi \end{bmatrix} \tag{36}$$

where again all forces are measured with respect to the xy plane of Figure 6. The IAB's x and y forces result in an equal x and y forces on the head; the overall torque is proportional to the head orientation. When forces are applied along the line connecting diagonally oriented IABs (e.g. the lines connecting IAB_1 and IAB_3), there will be no net force on the head as the null space of the map becomes spanned by the vector

$$\begin{pmatrix} 0 & 0 & -\frac{\sin\phi}{\cos\phi} & -r & \frac{-\sin\phi}{\cos\phi} \\ -r & 0 & -r & 0 & -r \\ 0 & -r & \frac{\sin\phi}{\cos\phi} & 0 & \frac{-\sin\phi}{\cos\phi} \\ r & 0 & 0 & 0 & 0 \\ 0 & r & 0 & 0 & 0 \\ 0 & 0 & r & 0 & 0 \\ 0 & 0 & 0 & r & 0 \\ 0 & 0 & 0 & 0 & r \end{pmatrix}. \tag{37}$$

C. Case III: Head Motion along xy plane and z

Consider the case where all 8 soft robots are actuated such that the head is raised to a height, h, on the treatment machine, and it is tilted along the xy plane as shown in left figure of Figure 7. Suppose the orientation of the head is by an angle ϕ as in Figure 6. We now describe the manipulation map for the IAB-head system.

$$G_i(x,y,\phi) = \begin{bmatrix} \mathbf{I} & 0 \\ \hat{\omega}\begin{pmatrix} \pm r\sin\phi \\ \pm r\cos\phi \\ h \end{pmatrix} & \mathbf{I} \end{bmatrix} \begin{pmatrix} 1 & 0 & 0 \\ 0 & 1 & 0 \\ 0 & 0 & 1 \\ 0 & 0 & 0 \\ 0 & 0 & 0 \\ 0 & 0 & 0 \end{pmatrix} \tag{38}$$

so that

$$G(x,y,\phi) = \begin{pmatrix} 1 & 0 & r\cos\phi \\ 0 & 1 & -r\sin\phi \\ 1 & 0 & -r\cos\phi \\ 0 & 1 & -r\sin\phi \\ 1 & 0 & -r\cos\phi \\ 0 & 1 & r\sin\phi \\ 1 & 0 & r\cos\phi \\ 0 & 1 & r\sin\phi \end{pmatrix} \tag{39}$$

VI. Multi-IAB Dynamics

From the *determinism principle for stress* [15], the Cauchy stress $\boldsymbol{\sigma}$ at any point in a material at time t for any motion up to time t determines the stress response of the material for any arbitrary motion history up to and including time t. We will derive the dynamics of the IAB system in the *strain field of the deformation*. The potential and kinetic energy of the system are considered to be derived from the constitutive strain field relations that characterize the deformation. We now use Lagrangian deformation analysis to derive the dynamic equations of the continuum multi-IAB system of Figure 2.

The constitutive law which describes the macroscopic IAB material behavior with respect to a reference frame, T, at a time, t can be completely characterized by ten dependent variables viz., three components of the position vector, six component stress tensor variables (the shear and normal stress components), and the density, ρ, of the material [10, §4.1.1].

A. Lagrange's Equations

We are interested in the final position and orientation of the IAB as a whole rather than the system of particles that characterize a deformation at every time t. For a kinetic energy T and a potential energy V, the *Lagrangian,* L, of the system in generalized coordinates is the difference between the kinetic and potential energy, *i.e.*

$$L(\mathbf{r},\dot{\mathbf{r}}) = T(\mathbf{r},\dot{\mathbf{r}}) - V(\mathbf{r}). \tag{40}$$

The equations of motion for the pneumatic system is of the form

$$\frac{d}{dt}\frac{\partial L}{\partial \dot{\mathbf{r}}_i} - \frac{\partial L}{\partial \mathbf{r}_i} = \boldsymbol{\tau}_i, \quad i = 1,\ldots,m \tag{41}$$

where $\boldsymbol{\tau}_i$ is the torque acting on the i^{th} generalized coordinate. Written in matrix form equation (41) becomes

$$\frac{d}{dt}\frac{\partial L}{\partial \dot{\mathbf{r}}} - \frac{\partial L}{\partial \mathbf{r}} = \boldsymbol{\tau}. \tag{42}$$

It now remains to derive the kinetic and potential energies for the IAB material. Let the velocity of an IAB material particle $\mathbf{x}$ in the current configuration at time t be $\mathbf{v}(\mathbf{r},t)$, then the Eulerian velocity gradient tensor can be defined as

$$\boldsymbol{\Gamma} = \text{grad } \mathbf{v}(\mathbf{r},t). \tag{43}$$

The first law of Cauchy's law of motion will allow us to derive the balance of mechanical energy of the system. Multiplying equation (**??**) throughout by $\mathbf{v}(\mathbf{r},t)$, and abusing notation by dropping the arguments of $\mathbf{v}(\mathbf{r},t)$, we find that

$$\begin{aligned} &\text{div } (\boldsymbol{\sigma}^T\cdot\mathbf{v}) + \rho\mathbf{b}\cdot\mathbf{v} = \rho\mathbf{v}\cdot\dot{\mathbf{v}} \\ \implies &\text{div } (\boldsymbol{\sigma}^T\mathbf{v}) - \mathbf{tr}(\boldsymbol{\sigma}\,\boldsymbol{\Gamma}) + \rho\mathbf{b}\cdot\mathbf{v} = \rho\mathbf{v}\cdot\dot{\mathbf{v}}. \end{aligned} \tag{44}$$

Following mass conservation, we integrate over volume $\mathcal{B}$ and employ the divergence theorem, so that the above relation yields the *balance of mechanical energy*:

$$\int_{\mathcal{B}} \rho\mathbf{b}\cdot\mathbf{v}\,dv + \int_{\partial\mathcal{B}} f_\rho\cdot\mathbf{v}\,da = \frac{d}{dt}\int_{\mathcal{B}}\frac{1}{2}\rho\mathbf{v}\cdot\mathbf{v}\,dv + \int_{\mathcal{B}}\mathbf{tr}(\boldsymbol{\sigma}\,\boldsymbol{\Gamma})\,dv \tag{45}$$

where f_ρ is the IAB body force density, and the left hand side of the foregoing is the so-called *rate of working of the applied forces*. The symmetry of the stress tensor $\boldsymbol{\sigma}$ implies that $\mathbf{tr}(\boldsymbol{\sigma}\,\boldsymbol{\Gamma}) = \mathbf{tr}(\boldsymbol{\sigma}\,\boldsymbol{\Sigma})$ where $\boldsymbol{\Sigma}$ is given in terms of the Eulerian-strain rate tensor,Γ *i.e.*

$$\boldsymbol{\Sigma} = \frac{1}{2}(\boldsymbol{\Gamma} + \boldsymbol{\Gamma}^T) \tag{46}$$

so that the kinetic energy density and stress power are given by,

$$T(\mathbf{r},\dot{\mathbf{r}}) = \frac{1}{2}\rho\mathbf{v}\cdot\mathbf{v}, \quad V(\mathbf{r}) = \mathbf{tr}(\boldsymbol{\sigma}\,\boldsymbol{\Sigma}). \tag{47}$$

The stress-strain relation for the IAB we have presented are only related through the deformation tensor dependence, implying that the material is Cauchy elastic. For Cauchy elastic materials, the stress power term is not conserved during deformation making integration over the material body $\mathcal{B}$ physically unrealistic [10]. For such materials, we may set the stored strain energy V to an arbitrary constant (e.g. an identity or $V(I) = 0$). We can derive the overall torque dynamics of an IAB system as

$$\begin{aligned} \boldsymbol{\tau} = &\underbrace{\begin{bmatrix} \rho & 0 & 0 \\ 0 & \rho r^2 & 0 \\ 0 & 0 & \rho r^2\sin^2\phi \end{bmatrix}}_{M_{iab}} \begin{bmatrix} \ddot{r} \\ \ddot{\phi} \\ \ddot{\theta} \end{bmatrix} \\ &+ \underbrace{\mathbf{diag}\begin{bmatrix} 2\rho r\left(\dot{\theta}\sin^2\phi + \dot{\phi}\right) \\ \rho r\left(r\dot{\theta}\sin 2\phi - \dot{\phi}\right) \\ -\rho r\dot{\theta}\sin\phi\,(r\cos\phi + \sin\phi) \end{bmatrix}}_{C_{iab}} \begin{bmatrix} \dot{r} \\ \dot{\phi} \\ \dot{\theta} \end{bmatrix} \end{aligned} \tag{48}$$

Rewriting equation (48) in terms of the torque for each soft robot in Figure 2, we have the dynamics for IAB j as

$$M_{iab_j}(r_j,\phi_j)\ddot{\mathbf{r}}_j + C_{iab_j}(r_j,\phi_j,\dot{\theta}_j,\dot{\phi}_j)\dot{\mathbf{r}}_j = \boldsymbol{\tau}_j \tag{49}$$

where M_{iab_j} and C_{iab_j} are the respective inertia and Coriolis forces matrices for the soft robot, j while $\boldsymbol{\tau}$ is the actuator torque. Since the material of the IAB is incompressible, the mass density is uniform throughout the body of the material. In general, we write equation (49) as

$$\boldsymbol{M}_{iab}(\tilde{\mathbf{r}})\ddot{\tilde{\mathbf{r}}} + \boldsymbol{C}_{iab}(\tilde{\mathbf{r}},\dot{\tilde{\mathbf{r}}})\dot{\mathbf{r}} = \tilde{\boldsymbol{\tau}} \tag{50}$$

where $\tilde{\mathbf{r}} \in \mathbb{R}^{n_1} \times \mathbb{R}^{n_2} \times \cdots \mathbb{R}^{n_8}$ gives the generalized coordinates for all the IABs and $\tilde{\boldsymbol{\tau}}$ are the vectorized torques of the individual robots.

VII. System Newton-Euler Equations

The dynamics of the head is a form of (50) but without the actuator torques. In local coordinates, it has the form

$$\boldsymbol{M}_h(\zeta)\ddot{\zeta} + \boldsymbol{C}_h(\zeta,\dot{\zeta})\dot{\zeta} + \boldsymbol{N}_h(\zeta,\dot{\zeta}) = 0 \tag{51}$$

with ζ being a local parameterization of the position and orientation of the head, $x_h \in SE(3)$, and $\boldsymbol{N}_h$ being the gravitational and frictional forces. The head and the multi-DOF IAB system are connected via manipulation constraint *i.e.*

$$G^T(\zeta,\mathbf{r})\dot{\zeta} = \boldsymbol{J}(\zeta,\mathbf{r})\dot{\mathbf{r}}. \tag{52}$$

Suppose that the velocity constraint produces a virtual displacement constraint in $\delta\zeta$ and $\delta\mathbf{r}$ such that for $q = (\zeta, \mathbf{r})$, we have

$$\delta\mathbf{r} = \boldsymbol{J}^{-1}(q)G^T(q)\delta\zeta$$

the Lagrange equations become

$$\left(\frac{d}{dt}\frac{\partial L}{\partial \dot{q}} - \frac{\partial L}{\partial q} - (\boldsymbol{\tau}, 0)\right)\delta q = 0 \tag{53}$$

$$\begin{pmatrix} \frac{d}{dt}\frac{\partial L}{\partial \dot{\mathbf{r}}} - \frac{\partial L}{\partial \mathbf{r}} - \boldsymbol{\tau} \\ \frac{d}{dt}\frac{\partial L}{\partial \dot{\zeta}} - \frac{\partial L}{\partial \zeta} \end{pmatrix}^T \begin{pmatrix} \delta\mathbf{r} \\ \delta\zeta \end{pmatrix} = 0 \tag{54}$$

$$\begin{aligned} \left(\frac{d}{dt}\frac{\partial L}{\partial \dot{\mathbf{r}}} - \frac{\partial L}{\partial \mathbf{r}} - \boldsymbol{\tau}\right)\delta\mathbf{r} + \left(\frac{d}{dt}\frac{\partial L}{\partial \dot{\zeta}} - \frac{\partial L}{\partial \zeta}\right)\delta\zeta = 0 \\ GJ^{-T}\left(\frac{d}{dt}\frac{\partial L}{\partial \dot{\mathbf{r}}} - \frac{\partial L}{\partial \mathbf{r}} - \boldsymbol{\tau}\right)\delta\zeta + \left(\frac{d}{dt}\frac{\partial L}{\partial \dot{\zeta}} - \frac{\partial L}{\partial \zeta}\right)\delta\zeta = 0 \end{aligned} \tag{55}$$

from where

$$\left(\frac{d}{dt}\frac{\partial L}{\partial \dot{\zeta}} - \frac{\partial L}{\partial \zeta}\right)\delta\zeta + GJ^{-T}\left(\frac{d}{dt}\frac{\partial L}{\partial \dot{\mathbf{r}}} - \frac{\partial L}{\partial \mathbf{r}}\right) = GJ^{-T}\boldsymbol{\tau} \tag{56}$$

given the arbitrariness of $\delta\zeta$. Equations (56) alongside (52) completely describe the system.

VIII. Conclusion

TO-DO: To be developed.

References

[1] O. Ogunmolu, X. Liu, and R. Wiersma, "Mechanism and Constitutive Model of a Continuum Robot for Head and Neck Cancer Radiotherapy." 1, 2, 3, 4

[2] O. P. Ogunmolu, "A Multi-DOF Soft Robot Mechanism for Patient Motion Correction and Beam Orientation Selection in Cancer Radiation Therapy." Ph.D. dissertation, The University of Texas at Dallas; The University of Texas Southwestern Medical Center, 2019. 1, 3, 5

[3] F. M. Khan, J. P. Gibbons, and P. W. Sperduto, *Khan's Treatment Planning in Radiation Oncology*. Lippincott Williams & Wilkins, 2016. 1

[4] J. Merlet, *Parallel robots*. Springer, 2015. 1

[5] F. Faure, C. Duriez, H. Delingette, J. Allard, B. Gilles, S. Marchesseau, H. Talbot, H. Courtecuisse, G. Bousquet, I. Peterlik, and S. Cotin, "SOFA: A Multi-Model Framework for Interactive Physical Simulation," in *Soft Tissue Biomechanical Modeling for Computer Assisted Surgery*, ser. Studies in Mechanobiology, Tissue Engineering and Biomaterials, Y. Payan, Ed. Springer, June 2012, vol. 11, pp. 283–321. [Online]. Available: https://hal.inria.fr/hal-00681539 2

[6] V.-D. Nguyen, "Constructing force-closure grasps," *The International Journal of Robotics Research*, vol. 7, no. 3, pp. 3–16, 1988. 2, 6

[7] D. J. Montana, "The Kinematics of Contact And Grasp," *The International Journal of Robotics Research*, vol. 7, no. 3, pp. 17–32, 1988. 2, 5

[8] M. Mooney, "A theory of large elastic deformation," *Journal of applied physics*, vol. 11, no. 9, pp. 582–592, 1940. 3

[9] A. Gent, *Engineering with Rubber. How to Design Rubber Components*. Munich: Carl Hanser Verlag Publicationbs, 2012. 3

[10] R. Ogden, *Non-linear Elastic Deformations*. Mineola, New York: Dover Publicationbs, Inc., 1997. 3, 4, 8

[11] O. Ogunmolu, E. Pearson, X. Liu, and R. Wiersma, "Kinematics and Dynamics of a Continuum Robot Immobilization Mechanism for Cancer Radiotherapy," *Submitted to IEEE Transactions on Robotics, 2019.*, 2019. [Online]. Available: scriptedonachip.com/downloads/Papers/ContinuumII.pdf 3

[12] M. Spivak, "A Comprehensive Introduction to Differential Geometry. Vol. V. Berkeley: Publish or Perish," *Inc. XI*, 1979. 5

[13] R. M. Murray and S. Sastry, "Grasping and Manipulation using Multifingered Robot Hands." in *Proceedings of Symposia in Applied Mathematics*, vol. 41, 1990, pp. 329–335. 5, 6

[14] J. R. Kerr, "An Analysis of Multi-Fingered Hands," *International Journal of Robotics Research*, no. Dept. of Mechanical Engineering, pp. 3–17, 1984. [Online]. Available: http://journals.sagepub.com/doi/pdf/10.1177/027836498600400401 6

[15] C. Truesdell and W. Noll, *The Non-Linear Field Theories of Mechanics*. Springer, 1965. 8